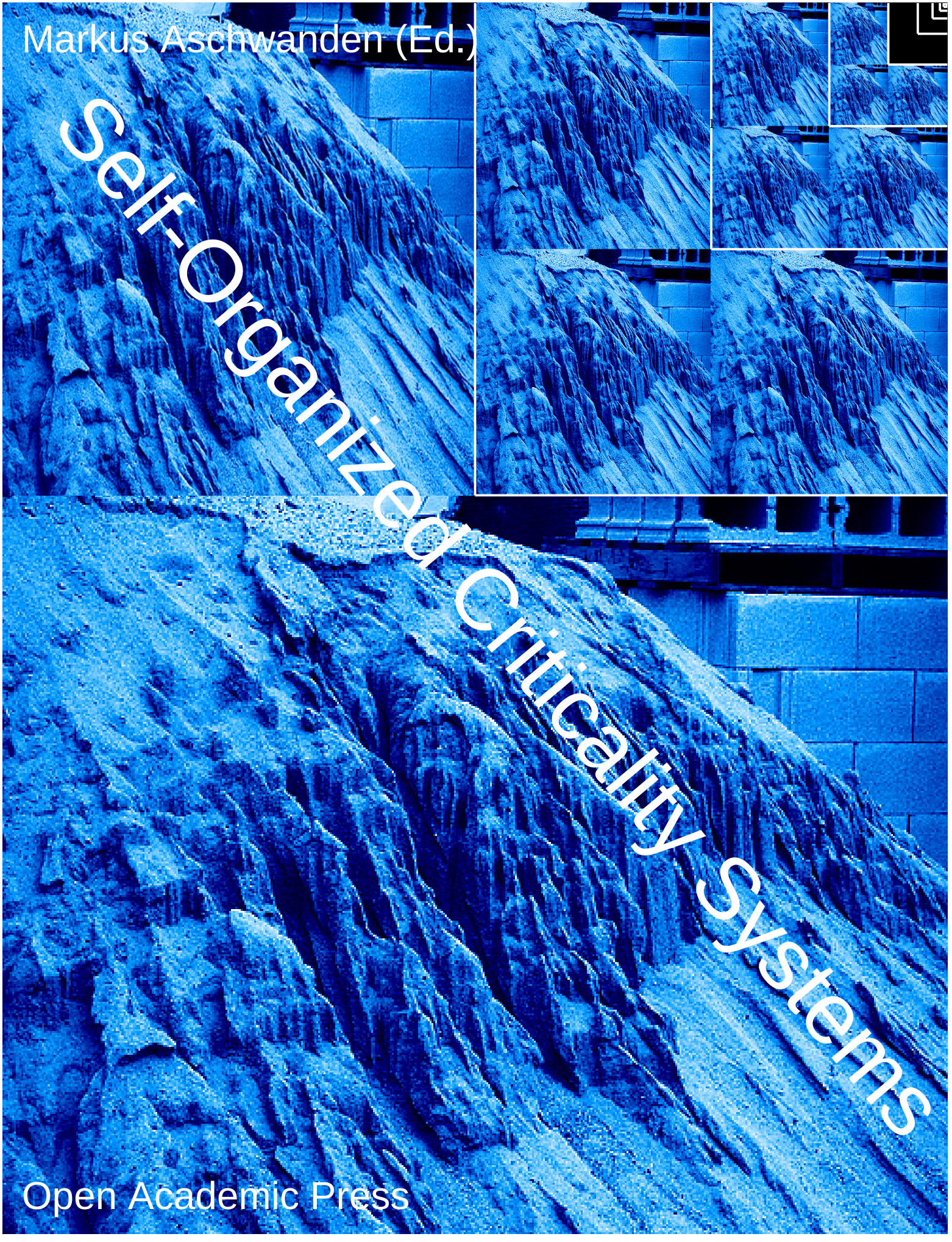
Markus Aschwanden (Ed.)
Self-Organized Criticality Systems
Open Academic Press

# Markus J. Aschwanden (Editor)

Open Academic Press Berlin Warsaw 2013

# Self-Organized Criticality Systems

Dr. Markus Josef Aschwanden (Editor)
Lockheed Martin, Advanced Technology Center
Solar & Astrophysics Lab, Dept., Org. ADBS, Bldg.252
3251 Hanover Street, Palo Alto, CA 94304, USA
Telephone: 650-424-4001, Fax: 650-424-3994
E-mail: aschwanden@lmsal.com

Published by Open Academic Press Berlin Warsaw 2013
Open Academic Press, Großbeerenstraße 2-10, 12107 Berlin, Germany
Open Academic Press/Villa Europa, ul. Sienna 64, 00-807 Warsaw, Poland

# Contents

# Chapter 3
# SOC and Fractal Geometry

R. T. James McAteer

**Abstract**

Clouds are not spheres, mountains are not cones, coastlines are not circles, and bark is not smooth, nor does lightning travel in a straight line -
Benoit Mandelbrot (1982).

When Mandelbrot, the father of modern fractal geometry, made this seemingly obvious statement he was trying to show that we should move out of our comfortable Euclidean space and adopt a fractal approach to geometry. The concepts and mathematical tools of fractal geometry provides insight into natural physical systems that Euclidean tools cannot do. The benefit from applying fractal geometry to studies of Self-Organized Criticality (SOC) are even greater. SOC and fractal geometry share concepts of dynamic n-body interactions, apparent non-predictability, self-similarity, and an approach to global statistics in space and time that make these two areas into naturally paired research techniques. Further, the iterative generation techniques used in both SOC models and in fractals mean they share common features and common problems. This chapter explores the strong historical connections between fractal geometry and SOC from both a mathematical and conceptual understanding, explores modern day interactions between these two topics, and discusses how this is likely to evolve into an even stronger link in the near future.

R. T. James McAteer
New Mexico State University, Department of Astronomy, Las Cruces, NM 88003 e-mail: mcateer@nmsu.edu

Self-Organized Criticality Systems - Dr.Markus J. Aschwanden (Ed.)

## 3.1 From chaos to order (and back)

Probably the most fundamental principle of the entire scientific process is that science and scientific laws are real, are within human understanding, are discoverable, and are universal. Self-Organized Criticality (SOC) is an excellent demonstration of this principal: it is a theoretical construct rooted in reality, discovered by simulations, and universally applicable across a diverse array of topics. SOC is introduced in Chapter 1 of this book; for the purposes of this chapter I would like to summarize it as a forced, non-linear, system that builds up energy via a series of interactions, eventually reaching a critical state at which energy dissipation naturally occurs. These systems tend to exhibit complex patterns in space and time. It is these complex patterns that we use to draw a connection to fractal geometry. It is important to note right from the beginning that although links can be drawn between SOC and fractal geometry, these links are not necessarily causal - i.e., any self-organization will lead to a fractal geometry system and hence SOC is only one such route to fractality.

An interesting historical link between SOC and fractal geometry, and their roles in the scientific process, can be drawn by looking back across human history. Every early form of society and religion have two aspects in common. From the Babylonians, to the Aztecs, to the Indigenous Australians - no matter which early society we look at, we see that they had a similar understanding of the sky (an early geometric cosmology) and of music (an early system of story telling). In his Pulitzer Prize winning book, 'Gödel, Escher, Bach', Hofstadter was one of the first to draw this link between differing forms of human perception and consciousness (Hofstadter, 1970). There are a number of common aspects between these two subjects of music and cosmology, and their link to human perception, which shed some light on the connections between SOC and fractal geometry. First, these early forms of cosmology tended to have an ordered universe appearing out of a disordered void. Early Proto-Indo-European religions often described the formation of the cosmos as the result of a clash between representatives of chaos and order, which of course resulted in a victory for order. It is no surprise that this concept of order appearing *ex-nihilo* has been retained in many modern religions. I discuss how this order-from-chaos applies to fractals and SOC in Section 3.1. Second, both these ideas of early cosmology and music are often considered as attempts by the human brain to force a classification of patterns out of the complexity and noise of everyday life. This classification was well defined by the early Greeks in the form of geometry - a concept that continued to dominate the minds of natural philosophers until the introduction of algebra and calculus in the seventeenth century. I connect fractal geometry to SOC by revisiting the study of geometry in Section 3.2. Third, everyone agrees when they hear beauty in music and see beauty in the sky, but in both cases beauty can often be difficult to quantify. This concept is famously summarized by as,

I shall not today attempt further to define the kinds of material I understand to be embraced within that shorthand description; and perhaps I could never succeed in intelligibly doing so. But I know it when I see it.
Justice Potter Stewart, Jacobellis v. Ohio, 1964.

I set the scene of *knowing it when we see it* by describing the many and varied attempts at quantifying fractal geometry in relation to SOC in Section 3.3. Fourth, modern cosmology and music show that things tend to be more complicated than at first glance. I discuss the complication of multifractals in Section 3.4, where I attempt to link multiple formulations of multifractality to those of turbulence. Finally, in Section 3.5, I revisit the progression of these studies of SOC and fractal geometry with a look forward at what these two connected branches of science may produce in the future.

### *3.1.1 The coffee table fractal*

In order to probe the connections between fractals and SOC it is useful to first of all study the historical setting of both phrases. In this historical context, fractals and fractal geometry are one of the few mathematical subjects to make the jump from pure abstract equations to the coffee table. In his popular 1982 book 'The Fractal Geometry of Nature' Mandelbrot showed that fractal geometry is universal and natural, occurring everywhere as the output of a system with some forced input and some simple rules (Mandelbrot, 1982). This same rules apply to SOC. The phrase *fractal* was derived slightly earlier by Mandelbrot in his 'Les objets fractals, forme, hasard et dimension' (Mandelbrot, 1975) from the latin *fractus*, meaning fractured or broken. Mandelbrot captured the public's imagination by showing how a simple iterative process can arrived at a complex and beautiful geometry. Just over a decade later in 1987 James Gleick authored another famous best-seller which made the jump from pure mathematics to popular science. In 'Chaos' (Gleick, 1987), Gleick showed the universal nature of chaos theory by demonstrating how a few simple iterative equations rapidly lead seemingly predictable systems into randomness - SOC exhibits a similar behavior of crashes when a critical threshold is met. This was further popularized by the movie 'Jurassic Park', one of the best examples of discussions of the ramifications of chaos theory in all of Hollywood.

The tyrannosaur doesn't obey set patterns or park schedules. The essence of Chaos.

This chaos can be interspersed by periods of order, only to revert back to chaos a few iterations later. It is important to recognize that both these modern subjects of fractals and chaos are connected to that of SOC under the larger and much older umbrella of *dynamics* - in each case we are simply posing the same question as Sir Isaac Newton in 'Principia Mathematica' (Newton, 1687) - How does a system change with time? This gives three potential connections between SOC and fractal geometry.

- Fractal geometry and SOC are both natural and universal.
- Fractal geometry and SOC both have simple inputs, but complex output.
- Fractal geometry and SOC both deal with the study of dynamics.

### *3.1.2 The n-body problem*

Newton made two definitions in Principia that remained unchallenged until Einstein's relativity, and still remain fundamental to studies of SOC and fractal geometry. He stated

> Absolute, true, and mathematical time, of itself, and from its own nature flows equably without regard to anything external. Absolute space, in its own nature, without regard to anything external, remains always similar and immovable.
> Isaac Newton, Principia Mathematica, 1687.

In doing so, he separated space and time. To Newton, space is a stage on which the universe acts, and time shows us how this acting occurs. Models of both SOC and fractals retain this by building a grid (of space) and studying how 'particles' behave in time. Newton famously went on to make numerous substantial contributions in science, including that of calculus. He showed that given sufficiently accurate measurements, he could accurately predict the future evolution of any system. Newton was able to the derive the equations of Kepler (the square of a planet's orbital period varies as the cube of its distance from the Sun) and Galileo (the acceleration of an object is independent of its mass) for any two body system. So Newton's laws could be, and still are, used to predict the Moon's orbit around the Earth, the Earth's orbit around the Sun, or a rocket's trajectory through the atmosphere. However, he also showed the limits of such studies. Try to analyze any three-body system (e.g., the Sun-Earth-Moon), or move to even greater numbers of bodies (e.g., the Sun-Earth-Moon-Rocket), and the equations are unsolvable. We cannot easily predict the position and velocity of more than two interacting bodies. The equations of such an n-body system are non-linear and unstable. Poincaré partially solved this quandary by restating the question in a different form (Poincaré, 1890). He showed that although we may not be able to predict the

position and velocity of each and every body, we can predict the statistical behaviour of such systems. Poincaré also took an early glance down the dark tunnel of chaos theory (although he did not call it 'chaos' as we know it today) by showing that the purely deterministic long term predictability of such an n-body system is impossible. This quick jaunt from Newton to Poincaré gives us three further features of fractal geometry that we can connect to SOC and which we study later in the chapter.

- Fractal geometry and SOC both rely on Newton's definitions of space and time.
- Fractal geometry and SOC both study the global statistics of the n-body problem.
- Fractal geometry and SOC inherently acknowledge that the long-term predictability of n-body systems is impossible.

### *3.1.3 The butterfly effect*

Despite the warnings of Poincaré, many scientists have had long and distinguished careers through the extended study of the n-body problem and non-linear dynamics. These pioneers include vander Pol and Andronov in the theoretical understanding of non-linear oscillators, Birkhoff in the 3-body problem, and Kolmogorov in the the study of turbulence. As is often the case, we can trace the next big breakthrough to the invention of a new piece of technology. In this case the creation of the computer in the 1950s, and the adoption of this by many industries, rapidly led to a new level of understanding of non-linear dynamics. In 1961 Lorenz was modeling the Earth's atmosphere to try to predict the weather, and found that he could not even successfully predict the known behavior in his models. He painstakingly tracked this back to round-off errors in the fourth decimal place of his numerical calculations. These small, seemingly insignificant, errors were creating dramatically different weather patterns in the future behaviour of his models. This is famously coined the 'butterfly effect' where a butterfly flapping its wings in London can eventually cause a storm in Tokyo, and the phrase symbolized the futility of such efforts in weather prediction. However, he also showed that if he plotted the behavior of such a system in an appropriate phase space, the resulting plot would be fractal (the famous strange attractor).

Mandelbrot went on to show that fractal geometry exists everywhere in space and time, from the coast of Norway to the patterns of shells to the shapes of galaxies, and from the behavior of cotton prices to population growth to stellar formation rates. In fact, far from being merely curious and fun (if somewhat unintuitive), fractal geometry is actually the more natural way of describing Nature (Mandelbrot, 1982). Mandelbrot showed that fractal patterns appeared at every possible scale, no matter how much he zoomed into, or zoomed out from, the data. He also described two types of

behavior with clear links to SOC: the Joseph effect, where a seemingly persistent regular series of values is suddenly interrupted; and the Noah effect where massive discontinuities occur on top of a series of noisy data. More than this, Mandelbrot popularized this field, and undoubtably his influence had a Joseph effect on this subject field itself. From a pedagogical perspective, the sort of burst in research activity driven by Mandelbrot's work is a perfect example of an episodic period in revolutionary science as popularized in Kuhn's 'The Structure of Scientific Revolutions' (Kuhn, 1967), which itself is now considered to have had a Joseph effect on the progress of science research. The work of Lorenz and Mandelbrot gives us three further points of emphasis to connect fractal geometry and SOC.

- No matter how seemingly unpredictable any non-linear dynamic system (including SOC) may appear, it can be described by fractal geometry when plotted in the appropriate phase space.
- A snapshot of the spatial distribution within any SOC system may be described by fractal geometry.
- The global dynamic evolution of an SOC system may be described by fractal geometry.

### *3.1.4 The critical points*

The rapid growth and interdisciplinary nature of chaos and fractal geometry in the 1970s and 1980s included many breakthroughs in physics (e.g., Hohenberg, 1971; Swinney & Gollub, 1978; Wolf et al., 1985), biology (e.g., Winfree, 1980), , and probability (e.g., Shaw, 1984). From the perspective of SOC studies, the most important work resulting from this period of rapid discovery was the Bak et al. (1987) paper. They proposed SOC as a mechanism for creating complexity in any natural system. This sandpile model, as described in this book, contains the concepts of self-similarity and scale invariance (described in Section 3.2.2) prevalent throughout studies of fractal geometry. Of course, when studying any natural system by experiments, such scale-invariance must have a lower and upper limit, whereas the previous work in pure mathematics is not restricted to such real world nuances. Further, when combined with Mandelbrot's work, it was clear that the onset of the critical point in these sandpile models resulted in power laws and scale-invariance, which could therefore be well described by fractal geometry in both space and time. However, it is important to realize that this is not the only route to fractal geometry (indeed any self organization naturally leads to power laws and fractal geometry).

The cellular automaton models, as described in this book, showed that the emergence of these critical points is a natural consequence of the system and will always arise no matter what the initial input. Note this non-sensitivity to initial conditions does not disagree with the butterfly effect - the sandpile

models merely showed that critical points will eventually arise, but it does not predict when they will arise. This period of recent development in the fields of SOC and fractal geometry leads us to the final important connections between these two subjects.

- Self similarity and scale invariance are both key aspects of SOC and fractal geometry, and these are statistically linked by power laws.
- Nature provides an upper and lower limit to these power laws that may be absent when presented as pure mathematics.
- Iteratively generated models (including cellular automaton models), are intrinsically fractal. Hence we can connect SOC theories and fractal theories via the study of these models and their application to natural phenomena.

## 3.2 Fractal Properties

The concept of fractals was conceived in mathematics but has now been so well assimilated into everyday language that its definition is now more commonly non-mathematical. Mathematically, we define a fractal as a set with a fractal dimension which exceeds it topographical dimension, i.e., a set of 0-dimensional points that as a whole is closer to a line, or a 1 dimensional line that is so complex that it is closer to a plane. In this description the topographical dimension is the dimension of the underlying basic shapes that make up the fractal, and the fractal dimension describes the overall complexity, or space-filling nature, of the system. In mathematical terminology, fractals are described by equations which are nowhere differentiable. This definition leads us down the route to non-integer exponents, providing a link to SOC described in Section 3.2.1. In this section we use the similarity dimension in the calculation of the fractal dimension and leave other definitions to Section 3.3.

Fractals are more commonly, and just as accurately, described and comprehended by any lay person without requiring knowledge of abstract mathematics. It is generally defined from a geometrical perspective as a shape each part of which exhibits the same statistical characteristics as the whole, a feature known as self-similarity (Section 3.2.2). In more simple language, a fractal is a shape made up of smaller copies of itself. This creates the scale-free nature of fractals, well described by a power law, and hence the many connections to SOC. It is however important to realize that although all fractals are self similar, not all fractals are the result of an SOC process. This concept of self-similarity leads to the second layman definition of a fractal as a shape which has been generated by an iterative process (Section 3.2.3). By starting with a simple shape, and applying a simple rule, it is trivial to form a fractal. This process leads to the well known coffee-table fractals such as the Sierpinksi carpet and the Koch snowflake. Many cellular automaton

models are generated by the same simple iterative process, hence we expect another close connection between SOC and fractality.

### *3.2.1 Dimensionality*

Classically, we define the dimensionality of an object as the number of independent directions, or the degrees of freedom, at the smallest scale. Hence, we see a point a 0-Dimensional, a line as 1-Dimensional, a drawing or sketch as 2-Dimensional, and a ball or cube as 3-Dimensional. This basis for Euclidean geometry, as defined over 2000 years ago in Euclid's 'The Elements', described everything that existed and was considered the only geometry possible until the discoveries of non-Euclidean space as epitomized by Einstein in the early twentieth century. One way of calculating the dimensionality of any object is to cover the details of the object with smaller and smaller similar objects and count how many of the smaller objects are required to entirely cover the original object at each size. One commonly used method which explains this well is as follows. Take a line of unit length and double it. Clearly it now takes two of the original lines to cover the new line. Now lets take a square of unit size and double it. This makes the square twice as wide and twice as high, so we require four of the original squares to cover it. Try a cube of unit size and double it so it is twice as wide, twice as high, and twice the depth. It will now take eight of the original cubes to cover it. The power of this simple experiment is clear by looking at the results in a table format

Table 3.1: The connection between dimensionally and scaling exponents becomes clear when presented in this Table. $N$ is the number of unit-sized objects required to cover the double-sized object, and $d$ is the dimensionality

| Shape | N = $2^d$ | Dimension |
|---|---|---|
| Line | $2 = 2^1$ | 1 |
| Square | $4 = 2^2$ | 2 |
| Cube | $8 = 2^3$ | 3 |

It is immediately apparent that the Euclidean dimension of an object is equal to the exponent of the scaling factor. This works for any scaling factor including non-integers - try changing the scaling factor to e.g., 3.5, or 1/5 and it will still work. If we move from simple Euclidean shapes to more complex shapes, the analogy seems to fall apart. The most famous example of this is an image of the coastline of Norway. If we use 2-Dimensional boxes to cover an image of this coastline, count them, scale the box, cover the coast with the rescaled boxes, count them, and proceed to rescale the box over and

over we arise at an equation with an exponent of $d = 1.52$. Seemingly the coast is neither 1- or 2- Dimensional. Instead its dimensionality is greater than that of a line, but less than that of a filled-in shape. Interestingly, other countries with smoother coastlines also have non-integer values, albeit much smaller (Coast of Britain $d = 1.25$, Coast of Australia $d = 1.13$). Clearly the fractal dimension of an object is in some way linked to its smoothness (or, in reverse, its spikiness). Fractals give us insight into the complexity of objects that Euclidean dimensions cannot.

We can conceptually connect this to the mathematical definition of differentiation. For example, a curve is differentiable is we can take a gradient at any point along it. However, for a spiky curve there may be locations where the gradient cannot be defined. Now imagine a curve that is spiky everywhere (e.g., the Weierstrass function), one that no matter how many times you zoom in to try to take a derivative, it turns out to be impossible. This curve is, by definition, fractal. These two concepts of dimensionality and differentiability are fundamental to the subject of fractals (Section 3.3.3).

### *3.2.2 Self-similarity and Scale-Invariance*

In nature, we are often confronted with objects with levels of complexity and detail at all scales. Fractal geometry can be used to examine the complexity of these objects across scales. Mathematically, an object is self-similar if it is exactly similar to some part of itself. In nature, few objects are exactly self-similar, but there exists a large family of objects which are statistically self-similar. In the discussion of the the coastlines of countries above we do not expect that the coastline of any part of Norway will look exactly like a miniature form of Norway. Instead it means that, upon zooming into a map of Norway, this zoomed in region will have a number of sharp curves and bends. The statistical distribution of these (i.e., the relative number of sharp curves and smoother bends) will be exactly the same as the country as whole. This form of statistical self-similarity is a typical property of fractals. In comparison, SOC often contains a very specific form of self similarity known as scale invariance, where at any magnification the smaller part of an SOC system is similar to the whole. Hence while a SOC system is always fractal, a fractal system is not always SOC.

### *3.2.3 Generating Fractals*

There are a number of different ways of generating fractals, but by far the most common is that of iterative generation. Here we describe the Cantor set,

the von Koch curve, and how we can solve the inverse problem of describing the rules of generation, given one snapshot in time.

#### 3.2.3.1 The Cantor set and the von Koch curve

The Cantor set is easily formed and contains many interesting facets in a comparison to SOC. It is constructed by starting with a number line containing every possible number between zero and one. Delete the middle third of this number line, but leave behind the end points. This produces two segments, of length 1/3, at each end. Now delete the middle third of each remaining segment, and repeat this operation ad infinitum. The remaining set of numbers at the limit of infinite iteration is the Cantor set. It will be an infinite number of infinitesimally small pieces, with lots of gaps. There are a number of important features of this set from which we can draw parallels to SOC. No matter how many times you zoom into this Cantor set, you will continue to see some structure. Second, it is scale invariant - by zooming in one level and moving to the outside third of the set you will see exactly the same structure as the parent. Third, its fractal dimension is an non-integer, and much higher than 0 (it is actually 0.63). SOC systems are often generated using a similar form of iterative generation, and often exhibit the same precise features of infinitely small structure, scale-invariance, and non-integer exponents.

The von Koch curve is generated by starting with some straight line segment. Remove the middle third and replace it with two sides of an equilateral triangle of the same length as the deleted segment. The resulting curve will have four segments, each length 1/3, for a total length of 4/3. Now repeat this same operation on each segment. The resulting curve from this step will have a length of $(4/3)^2$. Repeat this ad infinitum, and the curve obtained at the infinite iteration is the von Koch curve. The curve will have infinite length $(4/3^{\text{inf}})$ and the arc length between any two segments on the curve is infinite. Its fractal dimension is 1.26. As in the Cantor set, this contains structure at all size scales, is scale-invariant, and has a non-integer fractal dimension. The von Koch curve also shows the problems with trying to use traditional tools in the study of such SOC systems - if we tried to measure the length (or area) of the von Koch curve, we would find it is, rather disturbingly, infinity.

#### 3.2.3.2 Iterative Generation

Iterative generation is a powerful tool for generating a large number of fractals, but is readily explained from a few simple geometric descriptions. The iterative generation of any fractal, including the Cantor set and von Koch curve, is a combination of scaling, reflection, rotation, and translation. Take a simple 2-Dimensional seed shape, where any location of point can be described by its position along an x-axis and a y-axis. Scaling is then the mul-

tiplicative factor in either or both of these directions. Denote these scalings as x' and y', where $x' > 1$ corresponds to an increase in scale and $x' < 1$ corresponds to a reduction in scale. If the scaling is the same in both directions $(x' = y')$ , then the resulting fractal will be scale-invariant, otherwise it will be stretched or squashed in each direction. Reflection is described as a sign on the scaling factor, e.g., negative x' means a reflection in the x-axis. Reflection introduces two new components in our transformation matrix. Now, let $\theta_x$ be the rotation angle of any horizontal line, and $\theta_y$ be the rotation angle of any vertical line. Note that $\theta_x = \theta_y$ provides the conditions to retain scale invariance, otherwise the resulting shape will be stretched or squashed. Finally let $\Delta_x$ be a translation along the x-axis and $\Delta_y$ be a translation along the y-axis, where by convention up and to the right is positive. These parameters forms a matrix of scaling, reflection, rotation, and translation that prescribe all the freedom necessary to create any fractal shape. Start with the seed shape, apply the transformations in order to generate the second shape, then apply the transformation again to each new segment and repeat. The key link to SOC systems is that this matrix of transformation is usually all that is required to build any self-organized system. For instance, in a simple cellular automaton model, one may simply start off with equi-spaced particles and let them evolve according to some set of rules regarding their position and velocity. Although I described this here using a 2-Dimensional example, this can be extended to any number of dimensions in space and time.

#### 3.2.3.3 The inverse problem

The inverse problem seeks to carry out the reverse procedure to the iterative generation. That is, given the data (position, velocity) of the particles in the system under study, can we calculate the transformation matrix and hence deduce the rules governing the system. As such, the inverse problem is more familiar to most scientists dealing with observational data. In classical mechanics we can analytically solve the inverse problem for a small number of bodies or simple geometry. In simple fractals the inverse problem consists of calculating the matrix which created the fractal geometry. For example the classical snowflake is widely known to have a simple 6-fold rotation symmetry and self-similar scaling. Directly solving for the transformation matrix is quite a powerful technique and can be used to infer the physics behind the generation of more complex fractals in nature, many of which may be the result of SOC, including the the architecture of trees and the classical spiral shape of sea shells and galaxies. Inevitably however, as we include more and more particles, we quickly run into n-body effects. Making an inference of the initial state and deciding on the rules which generated the geometry are almost impossible to obtain. Even if we can obtain such a set of rules, they are almost certainly not unique. In these cases, we can study the statistics of the system and see if it is possible to forward-fit an iteratively generated model to

reproduce these statistics (e.g, in diffusion limited aggregation, particles are modeled to undergo a random Brownian motion and cluster together to form aggregates and simulations can be done on lattices of any desired geometry.)

## 3.3 The many flavors of fractal dimension

It is instructive to introduce the main types of fractal analyses techniques and dimensions. Often the type of fractal dimension reported is a result of the technique used to obtain it so one must be very careful in cross-comparing any studies of fractal geometry or any comparison of data to models. Here we will introduce two methods of calculating the fractal dimension of both individual systems and a set of these systems, and then define the commonly used phrases of Hurst Exponent, Hölder exponent, and Haussdorff dimension. It is important to understand the similarities and the differences between each method. Further, it is also vital to consider that because of the finite nature of real data, any method can only ever represent an approximation to the actual fractal dimension of Nature.

### *3.3.1 Similarity Dimension of a set of systems*

One method to calculate the similarity dimension of any set of systems is by studying a measure of their 1-Dimensional size compared to their 2-Dimensional size. One such technique relates the perimeter lengths, $P$, of a large set of structures of different sizes to their areas, $A$, via the relationship,

$$P(A) \propto A^{D_{PA}/2} , \tag{3.1}$$

where $D_{PA}$ is the perimeter-area similarity dimension of the set of structures. For a simple geometric shape (e.g., a square with side of length $l$, $A = l^2$, $P = 4l$) $D_{PA} = 1$, whereas for the high perimeter limit (e.g., the same square filled, $A = l^2$, $P = l^2$) $D_{PA} = 2$. Hence $D_{PA}$ is an indication of the complexity of the perimeters of the set of structures and can be calculated from the two-fold slope of a plot of log $P$ versus log $A$ over the entire set of structures. In astrophysics this has been applied to solar granulation in broadband white light images leading to debate over the formation process of these convection features (Roudier & Muller, 1987; Hirzberger et al., 1997; Bovelet & Wiehr, 2001). A closely related study of small scale magnetic fields (Janssen et al., 2003) obtained a similar value of $D_{PA}$ from data and simulations, regardless of the spatial size (i.e., pixel scale) of datasets or the simulation.

The linear size-area technique differs by relating the minimum size of the boxes, $L$, which contain structures (or clusters of contiguous pixels), to their

area, $A$, via,

$$L(A) \propto A^{1/D_{LA}} , \tag{3.2}$$

where $D_{LA}$ is the linear size-area similarity dimension of the set of areas. In contrast to the perimeter-area method, for a simple geometric shape $D_{LA} = 2$, whereas for a more serrated shape, $D_{LA} < 2$. A plot of log $L$ versus log $A$ over the entire set of structures will provide an indication of the complexity of the set. This has been applied to sunspot magnetic fields (Lawrence, 1991; Balke et al., 1993) and compared to the predictions of percolation theory. Comparisons of both the perimeter-area and linear size-area methods (Meunier, 1999) to a large set of active regions showed that solar active regions may also be considered as the result of a percolation process at the bottom of the convection zone of the Sun, combined with a diffusion process at the surface. It is worth noting at this stage that such a percolation process is good example of self-organized process that is not fully SOC, but still gives rise to fractal geometry (Section 3.2.2)

### *3.3.2 Box Counting Dimension*

The box counting technique is similar to that described in Section 3.3.1 above, except it can be applied more readily to a single image, (whereas the previous techniques provide the fractal dimension of a set of images). The first step in such a technique is to threshold an image in intensity and thereby create a binary image. This binary image is overlaid with a series of grids consisting of successively larger boxes. The number of boxes, $N$, containing any part of the binary image scales with box size, $\epsilon$, as

$$N(\epsilon) \propto \epsilon^{-D_{BC}} , \tag{3.3}$$

where $D_{BC}$ is the box counting fractal dimension. The implications of this definition are discussed further in Section 3.3.5, but to complete the comparison to the previous two methods, a simple non-fractal geometric shape will have $D_{BC} = 1$, whereas a non-fractal filled area will have $D_{BC} = 2$. Two extensions of this technique - the Jaenisch and differential box counting methods (Stark et al., 1997) - are designed to overcome the issues with the conversion of the data in the thresholding and the limits of the fractal scaling. The box counting technique can also be extended to provide a multifractal measure (Section 3.4), albeit with significant provisos and problems. The biggest problem in using this technique lies in choosing the threshold value. In a rather simple sense it is possible to threshold the image at different levels of intensity. For standard fractal geometry the resulting calculation of $D_{BC}$ will not vary as a function of intensity thresholds. A change in fractal dimension with changing threshold is often associated with the existence of a structure more complex than a simple fractal.

### 3.3.3 The Hölder Exponent

Section 3.2.1 introduced the connection of differentiability and fractal geometry. Here we extend this concept by providing a mathematical formalism related to singularities. Singularities are those points where it may not be possible to take a derivative. However, they can still be studied and quantified by analyzing their Hölder Exponent, $h$. Let $f(x)$ be a function defined on the real number line, and let $\alpha$ be a real positive number. The function $f$ is defined to satisfy the Hölder condition if both $C$ and $\alpha$ exist such that we can find a polynomial $P_m$ of degree $m$, no greater than the integer part of $\alpha$, such that for all $x$ in the neighborhood of $x_0$

$$|f(x) - P_m(x - x_0)| \leq C|x - x_0|^{\alpha} \ . \tag{3.4}$$

Given this, the pointwise Hölder exponent of the function $f$ at $x_0$ is defined by

$$h(f, x_0) = \sup \{\alpha > 0 | f \in C^{\alpha}(x_0)\} \ , \tag{3.5}$$

that is, the Hölder exponent is the least upper bound such that $f$ belongs to $C^{\alpha}(x_0)$. Consider the following example functions (Seuret & Gilbert, 2000; McAteer et al., 2007),

$$\mathrm{f}_1(x) = \begin{cases} -|x|^3 & \text{for } x < 0 \\ |x|^2 & \text{for } x \geq 0 \end{cases} \ ,$$

$$\mathrm{f}_2(x) = \begin{cases} -|x|^3 \sin(1/x^2) & \text{for } x \neq 0 \\ 0 & \text{for } x = 0 \end{cases} \ .$$

Both functions exhibit sharp changes as one approaches $x = 0$. Note that the derivative of $f_1$ is continuous at $x = 0$, but that the derivative of $f_2$ is not defined at $x = 0$. However, for both functions, the Hölder exponent at $x = 0$ is 2 ($h(f, 0) = 2$), since one can write $|f_1(x) - x^2| \leq |x|^2$ and $|f_2(x)| \leq |x|^2$ in this neighborhood. Hence the Hölder exponent permits the characterization of singularities in a series of values, regardless of whether the derivative exists at that point, and provides a powerful technique of calculating the fractal dimension.

### 3.3.4 The Hurst Exponent

This idea of describing the spikiness (or smoothness) of a function was introduced by Mandelbrot (1982). This work in probability theory originates back to the pioneering work of Robert Brown in 1827, who described the random nature of the motion of pollen grains under his microscope. Mandelbrot defined fractional Gaussian noise as the increments of this Brownian motion phenomena and showed that fractional Gaussian noise signals can be charac-

terized by the Hurst exponent, $H$. Where $c$ is a constant and $f(x)$ is a fractal process, $g(x) = f(cx)/c^H$ is also a fractal process, moreover it maintains the same statistical distribution. The calculation of the Hurst exponent involves an integration of the signal, therefore when compared to the Hölder exponent, $h = H - 1$. The Hurst exponent describes different types of signals. For Brownian motion, each step along the a series is unrelated to any previous values, the series is just as likely to increase as to decrease and hence we prescribe random white noise with a Hurst exponent of 0.5. Anti-persistent (non-stationary) noise has $0 < H < 0.5$ whereas persistent (stationary) noise has $0.5 < H < 1.0$. Pink noise is described by $H = 1.0$. For a bursty series which tends to show change (i.e., if the series is increasing, the next step is likely to be a decrease and vice versa), the curve covers less distance then a random walk, so $1.0 < H < 1.5$ and the series is described as an *anti-persistent* walk. For a smooth series (i.e., if the series is increasing, the next value will tend to be larger and vice versa), the curve covers more distance than a random walk, so $1.5 < H < 2.0$, and the time series is described as a *persistent* walk.

The Hurst exponent is also intrinsically related to the scaling index of the Fourier power spectral slope of the series. Provided the series is analogous to fractional Gaussian noise and where the Fourier spectral density of the signal scales as a power decay of index -$\beta$, then,

$$\beta = 2H - 1 = 2h + 1 \ . \tag{3.6}$$

This provides a powerful method for calculating the Hurst exponent and fractal dimension of any data. One can carry out an FFT, calculate the power spectrum, fit a slope to the energy spectrum and then back out the Hurst exponent. This could then be compared between SOC models and data. However caution is required in assigning strong conclusions to any such study as there are least a dozen methods of calculating the Hurst exponent (Clegg, 2009; Taqqu et al., 1995), and they can differ significantly in their solutions. This is particularly true when calculating the Hurst exponent in data where the intrinsic physical timescale of the system may be much smaller than the resolution of the observations.

### *3.3.5 Haussdorf Dimension*

The description of the Haussdorff dimension provides a more mathematically rigorous and general description of the box counting dimension above (Section 3.3.2). Consider $N(r)$ as the number of balls, radius $r$, required to cover a n-dimensional signal. As $r$ decreases, $N(r)$ increases such that

$$N(r) \propto \frac{1}{r^D} \ . \tag{3.7}$$

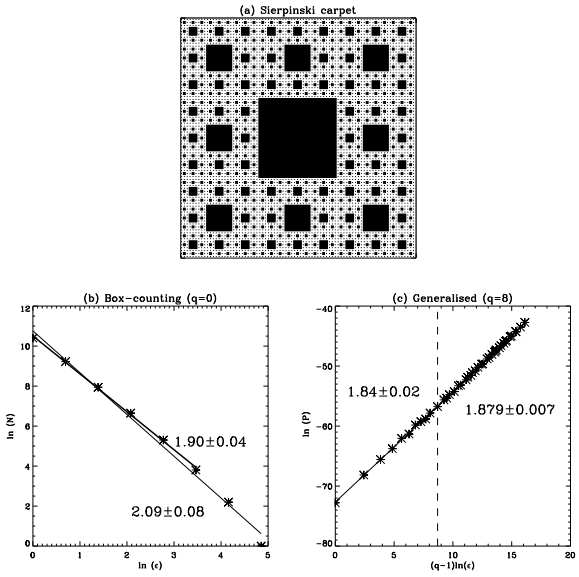


Fig. 3.1: The Sierpinski carpet (top, reproduced from McAteer et al., 2005) is a iteratively generated fractal that highlights the difficulties in calculating the fractals dimension using standard box counting (bottom left) and the possible solutions that can be used to obtain a more accurate determination of its fractal dimension (bottom right)

The Hausdorff-n dimension is then defined as

$$D = -\lim_{r \to 0} \frac{\log N(r)}{\log r} \ . \tag{3.8}$$

The box counting dimension is a version of the Haussdorf dimension implement with boxes rather than circles.

Typically the Hausdorff dimension is the same as the topographical dimension. However, for a fractal the Hausdorff dimension is strictly greater than its topographical dimension (i.e., a seemingly 1-Dimensional fractal curve is so complex, it can be thought of as occupying space closer to 2-Dimensional). For example, a simple straight line on a plane has a Hausdorff dimension of one. But consider a more complex object like the Sierpinski carpet (Figure 3.1) that is a more complex object than a simple line but where it is also clear that it does not fill up the entire plane; the Hausdorff dimension of the Sierpinski carpet is approximately 1.89. Of course for real data it is impossible to approach the limits of $r \to 0$ and so typically Equation 3.8 is described by plotting over a *linear range* of $r$. In this case the (normally square) image of side length $S$ is covered with grids of boxes with increasing side length $\epsilon$ ($\epsilon$ belongs to the set $2^n, n = 0, 1, 2, 3...$ such that $\epsilon_{max} = S$)

and $N(\epsilon)$ is the total number of boxes required to cover the image at each box size. The gradient of a straight line fit to the linear section of a plot of log $(N(\epsilon))$ against log $(\epsilon)$ corresponds to the fractal dimension. However this simplistic methodology is known to suffer from a poor fit to the log-log plot and so is prone to large errors. This problem is due to the inability of the grid to adequately describe the image at box sizes larger than one pixel, the small number of points in the linear range (a CCD size of $1K \times 1K$ pixels will only have 10 box sizes, $\epsilon_{max} = S = 2^{10}$, therefore the linear range could be as few as $6 - -7$ points), and the often dismissed requirement to rotate the images.

The results of these problems are presented here by studying the Sierpinski carpet in detail. This fractal is created by starting with a uniformly filled square, divided into nine smaller congruent squares, and the interior square removed (i.e., the 8 cells at the edges are uniformly filled with 1 and the centre cell is set to 0). This operation is then repeated on the 8 smaller squares iteratively until no further division can be carried out (the single pixel limit is reached). The resulting fractal has a fractal dimension of $\sim$1.8928 (=log(8)/log(3)). A simplistic box-counting algorithm produces the plot in Figure 3.1b. Although the shape is fractal, the log($N$)–log($\epsilon$) plot appears concave - a multifractal signature (Section 3.4). Over the entire range of scales, the fractal dimension is calculated as $2.09 \pm 0.08$ . Judging by eye, there appears to be a break at a box size of 32 pixels, and the gradient of the curve over the box size range of 1–32 pixels gives a much better estimation $(1.90 \pm 0.04)$ of the true fractal dimension.

There are a few steps which we can implement to circumnavigate these problems (McAteer et al., 2005; Lawrence et al., 1996). At each box size, $N(\epsilon)$ is calculated as the *minimum* number of boxes required to cover the image. This is achieved by translating the grid to every possible origin (e.g., a grid of boxes of side $\epsilon = 3$ will have 9 different possible origins). This should be repeated for every orientation of the image, but the obvious difficulties in precisely rotating a pixel array by any non-90 degree amount make this rotation difficult once the data is in this form (this should ideally be carried out in experiment by rotating the camera and taking snapshots at each rotation). In addition we can remove the $2^n$ box size dependence (which was really only introduced to decrease computation time) and remove the need to have square boxes (i.e., for a rectangular box of sides $a$ and $b$, the effective box size is $\epsilon_{eff} = \sqrt{ab}$).

This dramatically increases the number of data points at small box size (note the large number of data points in Figure 3.1c), hence we can introduce an quantitative indication of the linear section of the fit. For $L$ effective box sizes we carry out a linear fit to the log-log plot in a sliding window of size $l$ $(L/2 \leq l \leq L)$. At each position of the window, the fit is accepted if the spread in the fit in small; a window with a significant non-linear contribution will produce a large spread. This is displayed in Figure 3.1c where a fit over the entire range of box sizes produces a fractal dimension of 1.84$\pm$0.02 (an

underestimation of the true fractal dimension). A fit over a smaller section of the curve produces a fractal dimension of 1.879±0.007 (a much better estimation of the true fractal dimension), hence this section contains less of the non-linear range. Note I have also adopted a higher order moment in calculating the value Figure 3.1c), an approach borrowed from the study of multifractals.

## 3.4 Multifractals

It is entirely possible that any given signal will contain many different singularities strengths (Hölder exponents) at many different positions. For a signal with infinite resolution (or at least resolution smaller than any physical event) it would be possible to measure the Hölder exponent of each event and create a number density histogram to reflect the different numbers of each exponent. However when singularities are not isolated, as is generally the case for real data, one may calculate the Hausdorff dimension of the different singularities in the data. In this case, the Hausdorff dimension provides the necessary *statistical mechanics* approach to describing the number density of each Hölder exponent and performs the role of quantifying the degree with which a particular Hölder exponent is evident in a signal. For example, if the Hausdorff dimension of a particular Hölder exponent was 1, this would mean that the singularity of this type is evident everywhere in the time series. This naturally leads onto the topic of multifractals - shapes with a fractal geometry more complex than that of simple fractals. Although fractals are useful for quantifying the space-filling nature of any n-dimensional system, it has been found that many systems in nature are a convolution of different fractal processes. A multifractal exists when the measure itself is self-similar (Evertsz & Mandelbrot, 1992), and is usually described as a concave curve known as the singularity spectrum, $f(\alpha)$. If we are to make a comparison between SOC and measures of fractal geometry we must ensure we address this issue of multiple fractal processes within one signal. In this section I will expand on this discussion, with particular emphasis on the generalized dimensions, turbulence, and on the wavelet transform.

### *3.4.1 From monofractals to multifractals*

Section 3.3 showed that the fractal dimension of any object can be thought of as the self-similarity of a signal across all scale sizes. For any 2-Dimensional image this can be described as the scaling index of any length to area measure,

$$A \propto l^{\alpha} \ , \tag{3.9}$$

where $\alpha$ is the singularity strength. However, a multifractal system will contain a spectrum of singularity strengths of different powers,

$$A \propto l^{f(\alpha)} \ , \tag{3.10}$$

and takes account of the measure at each point in space. In Section 3.3.2 a fractal measure was obtained by thresholding in intensity and creating a binary image, hence the value of the measure in each pixel was lost. The route to producing multifractal measures starts with retaining these pixel intensities in the form of a measure distribution. In general, the measure distribution is characterized by

$$\psi(q,\tau) = E\sum_{i=1}^{N} P_i^q \epsilon^{-\tau} \ , \tag{3.11}$$

where $q$ and $\tau$ can be any real numbers, and E is the mean value of the measure with N components. In this form, $\psi$ is the coupled $\tau$ -moment of the size $\epsilon$, and $q$-moment of the measure $P$. The three main multifractal indices commonly used to represent a non-uniform measure are then the:

- generalized dimensions Grassberger & Procaccia (1983), $D_q = \tau/(q-1)$;
- singularity strength, $\alpha = d\tau/dq$;
- legendre transformed $f(\alpha) = q\alpha - \tau$ / .

When applied via a traditional box-counting approach, it is useful to define the partition function,

$$Z_q(\epsilon) = \sum_{i=1}^{N} P_i^q(\epsilon), \tag{3.12}$$

such that $\tau(q) = lim_{\epsilon\to 0} log(Z)/log(\epsilon)$, and any of the three representations above can be calculated. The $q$ moment plays the role of increasing the relative importance of the more intense parts of the measure as $q$ is increased. In this way it acts as a microscope to investigate the different contributions made to the image at higher values of the measure.

### *3.4.2 Generalized Dimensions*

We can arrive at the multifractal spectrum by generalizing the previous concept of the Hausdorff dimension as a member of an infinite series of $q^{th}$ order dimensions. The classical generalized $q^{th}$ order fractal dimension, $D_q$, of any image is given (e.g., Grassberger & Procaccia, 1983; Hilborn, 2000) as,

$$D_q \ = \frac{1}{q-1} \ lim_{\epsilon\to 0} \frac{ln \ \Sigma_{i=1}^{n} P_i(\epsilon)^q}{ln \ \epsilon} \ , \tag{3.13}$$

where $q = -\infty, ..., +\infty$. For a shape consisting of $m$ pixels, $P_i$ is the probability of finding a pixel in the $i^{th}$ box (with a total of $n$ boxes) and is given by,

$$P_i(\epsilon) \ = \ \frac{m_i(\epsilon)}{m} \ , \tag{3.14}$$

for a total of $m$ points in the image: hence $P_i$ is a indication of the measure in the $i^{th}$ box.

A measure is defined as the magnitude of the values within an area, e.g., for an image it could be the sum of the pixel values within the box under study (compare this with the simple box counting approach where the actual pixel values are thrown out when the binary image is constructed at some chosen threshold.) Each measure is then normalized to ensure that the sum of all the measures is unity. The exponent $q$ is used to extract the information at each value of the measure - when $q$ is positive it magnifies the larger measures, dwarfing the smaller ones; when $q$ is negative it inverts the measures, thus enhancing the smaller measures and dwarfing the larger ones. The normalized measure is given as,

$$\hat{P}_\epsilon(i) = \frac{P_\epsilon(i)^q}{\Sigma_{(i=1)}^{N(\epsilon)} P_\epsilon(i)^q} = \frac{P_\epsilon(i)^q}{z_\epsilon(q)} \ , \tag{3.15}$$

where $z_\epsilon(q)$ is once again the partition function. The fractal strength $\alpha$ is then

$$\alpha(q) = lim_{\epsilon \to 0} \Sigma_{i=1}^{N\epsilon} \hat{P}_\epsilon(i) log_\epsilon P_\epsilon(i) \ . \tag{3.16}$$

Equation 3.16 provides the local fractal dimension for $P_\epsilon(i)$, and is a measure of the strength of the fractal dimension at that scale $q$. The full singularity spectrum $f(\alpha)$ is then given by repeating this over a range of values of $q$,

$$f(q) = lim_{\epsilon \to 0} \Sigma_{i=1}^{N\epsilon} \hat{P}_\epsilon(i) log_\epsilon \hat{P}_\epsilon(i) \ , \tag{3.17}$$

$$f(\alpha) = q\alpha - lim_{\epsilon \to 0} \Sigma_{i=1}^{N\epsilon} \hat{P}_\epsilon(i) log_\epsilon z_\epsilon(q) \ , \tag{3.18}$$

$$f(\alpha) = q\alpha - \tau \ , \tag{3.19}$$

where we now define $\tau = lim_{\epsilon \to 0} log_\epsilon E(z_\epsilon(q))$. So $f(\alpha)$ is a weighted sum of the log of the normalized measure to the base $\epsilon$.

### *3.4.3 Connecting forms of multifractality*

Although there are multiple descriptions of multifractality, they are readily connected by a few simple equations (McAteer et al., 2010). Here we formulate and connect the Haussdorff dimension, Hölder exponent, equations of thermodynamics, and structure functions.

#### 3.4.3.1 The Hausdorff dimension and Hölder exponent

As we see below in section 3.4.5, one approach to measure the multifractal dimension is to calculate the Hausdorff dimension, $D$, of each Hölder exponent, $h$ in a signal. The resulting $D(h)$ spectrum as calculated at each moment, $q$, is directly related to the $f(\alpha)$ spectrum as,

- $f(\alpha) = D(h_q)$ ,
- $h_q = \alpha - E_{dim}$ ,

where $E_{dim}$ is the Euclidean dimension ($E_{dim} = 2$ for an image).

#### 3.4.3.2 The link to thermodynamics

The multifractal spectrum is often generated from the Legendre transform of the scaling exponents of a signal using an analogy to the laws of thermodynamics. The $f(\alpha)$ singularity spectrum was originally introduced to provide a statistical description of the multifractal spectrum in a manner related to well known thermodynamic quantities. In this analogy with thermodynamics, $f$ is 'entropy', $\alpha$ is 'internal energy', and these are related via a Legendre transform to $\tau$ ('free energy') and $q$ ('temperature'),

$$\alpha = \frac{d\tau}{dq} \ , \tag{3.20}$$

$$f(\alpha) = q\alpha - \tau(q) \ , \tag{3.21}$$

and this can be further related to the spectrum of generalized dimensions,

$$D_q = \tau(q)/(q-1) \ . \tag{3.22}$$

As it is generally simpler to calculate the $D_q$ spectrum, this relationship can be used to produce the singularity spectrum (e.g., Vlahos et al., 1995). In this case, the signal is covered by boxes (of increasing size $l$) and it found that the $q$th moment of the measure (or probability of occurrence), $P$, in each box, $i$, scales as,

$$D_q(q-1) = \tau(q) = \lim_{l \to 0} \frac{\log \sum_i P_i^q(l)}{\log(l)} \ . \tag{3.23}$$

By further analogy with thermodynamics, the summation is known as the partition function where, as already describe earlier, positive $q$ will accentuate the large values, and negative $q$ will survive the small values, of the measure. The calculated $D_q$ is then Legendre transformed to calculate the multifractal spectrum. However, this method suffers from known problems of non-linear scaling and discontinuities in $D_q$. A second approach circumvents this problem by calculating the singularity in each box $i$, $\alpha_i = \log \ P_i(l)/\log \ l$. The histogram $N(l)$ then varies as,

$$N(l) \sim l^{-f(\alpha)} \ , \tag{3.24}$$

and $f(\alpha)$ can be directly calculated. Unfortunately this method is shown to be inaccurate due to slow convergence (Chhabra & Jensen, 1989).

#### 3.4.3.3 Structure Functions

Another method of calculating the multifractal spectrum is based on the structure function (Parisi & Frisch, 1985; Abramenko et al., 2002). This method consists of calculating the statistical moments of the field increments $S_q(r)$, as a function of separation, $r$ in order to determine the scaling exponents, $\zeta_q$,

$$S_q(r) \sim r^{\zeta_q} \ , \tag{3.25}$$

which are also directly related to the multifractal spectrum as (Muzy et al. 1993),

$$D(h) = qh - \zeta_q + 1 \ , \tag{3.26}$$

$$h = \frac{d\zeta}{dq} \ . \tag{3.27}$$

In equation 3.27, it is the deviation of $h$ away from a single value that signifies multifractality.

### *3.4.4 The Devils staircase*

It is instructive to look at a typical multifractal spectrum and discuss a few salient features. The $D(h)$ multifractal spectrum of a well-known multifractal, the devil's staircase (also known as the Cantor function), is displayed in Figure 3.2, and the basic properties are as follows.

- The Hölder exponent (abscissa), as described in Section 3.3.3 is the singularity strength. The Hausdorff dimension (ordinate), as described in Section 3.3.5 reflects the space-filling degree of each Hölder exponent.
- The concave shape is typical of many multifractal spectra. The left leg describes the fewer, larger amplitude, events, which correspond on large positive $q$, whereas the right leg reflects the more common, smaller, singularities described by large negative $q$.
- The Hölder exponent with the largest Hausdorff dimension is the most common singularity strength and can be approximated to the Hurst exponent of the entire series, ($h = 0.63$, $H = 1.63$). The Hausdorff dimension of this Hölder exponent, $D(h) = 0.61$, is the Capacity Dimension and quantifies the space-filling degree of this singularity: $D(h) = 1$ describes a signal

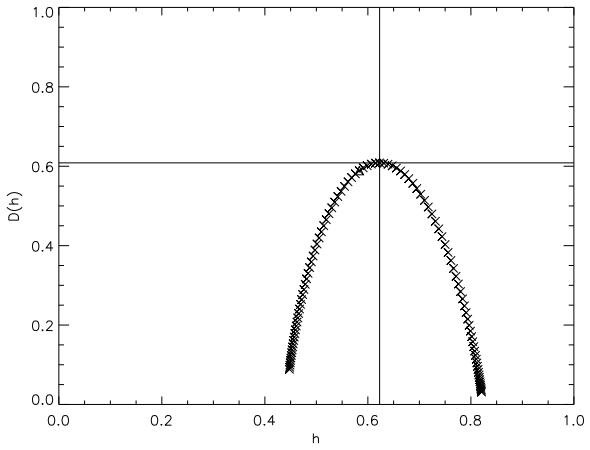


Fig. 3.2: The multifractal spectrum of the devil's staircase, represented as the Hausdorff dimension, $D$, of each Hölder exponent, $h$, exhibits the usual concave structure.

that is singular almost everywhere; $D(h) < 1$ describes a signal with rarer singularities.
- The spectrum exists over a range of Hölder exponents [$h_{min} = 0.47$, $h_{max} = 0.84$]. In the limit of monofractality, the spectrum would collapse to single point, only one Hölder exponent is necessary, and the range tends to zero.
- The degree of symmetry of the curve about $D(h)$ reflects the degree of inhomogeneity between rarer large amplitude and more common, small amplitude, singularities.

### *3.4.5 The Wavelet Transform Modulus Maxima*

The box counting technique (Section 3.3.2) has been applied successfully in multifractal studies (Lawrence et al., 1993; Cadavid et al., 1994) and a change in fractal dimension with scale (i.e., changing threshold) is often associated with the existence of a multifractal structure. However, it is important to note the difference between a true multifractal and the often observed sudden change of fractal dimension at large scales which may result from algorithm imperfections and/or data issues. A modification of this method to try to account for this is to randomly sample the image and renormalize the calculations (Cadavid et al., 1994). Other modifications include the Ĺ‡fuzzy ballĂ“ method (Alber & Peinke, 1997) which involves shaking the boundary of the box, and averaging over these local measures to obtain a more accu-

rate result of the true measure. However, there are know drawbacks to each of these methods. Box counting methods are known to be threshold dependent and structure functions are not defined for negative values of $q$. As such both methods are somewhat limited in their application to real data sets (Conlon et al., 2008, 2009; Georgoulis, 2005).

The continuous wavelet transform provided a new and natural method to overcome these issues and perform a complete multifractal analysis (Parisi & Frisch, 1985). The wavelet transform modulus maxima (WTMM) method replaces the boxes from the traditional box counting method with wavelets that act as fuzzy boxes, are defined for both finite and discrete domains, and are better suited for real data sets. Application of the WTMM method to 1-Dimensional time series have provided insight into a wide variety of problems, e.g., fully-developed turbulence, financial markets, meteorology, physiology, and DNA sequences (Muzy et al., 1991, 1993; Arneodo et al., 1995, 2002). The WTMM methods were generalized to 2 dimensions for multifractal analysis of rough surfaces and associated physical systems (Decoster et al., 2000) and to 3-dimensional turbulence dissipation data (Kestener & Arneodo, 2004).

The WTMM was formalized to overcome the algorithmic difficulties associated with Legendre transform methods and takes advantage of the large body of work carried out on the wavelet transform. The wavelet transform decomposes a N-dimensional signal $f(t)$ in both time and scale by the convolution of the signal with a set of dilated and translated wavelets,

$$WT(b,a) = \frac{1}{a^{N/2}} \int_{-\infty}^{\infty} \psi^* \left[ \frac{x-b}{a} \right] f(t) dt \ . \tag{3.28}$$

In this equation, $\psi^*$ is the complex conjugate of the mother wavelet, $a$ plays the role of adjusting its width, and $b$ shifts the wavelet along the signal. The mother wavelet is chosen to be well localized in both space and time, but furthermore if $\psi$ has $n$ vanishing moments, it can be shown that all polynomials up to order $n-1$ will be convolved to zero, thereby unmasking the local Hölder exponent by removing the $n-1$ polynomial trend. In the series of derivatives of a Gaussian,

$$\psi^n(t) = \frac{d^{(n)}}{dt^n} e^{\frac{-t^2}{2}} \ , \tag{3.29}$$

the first $n$ moments are vanishing. The wavelet power spectrum can be averaged over time to produce a global wavelet spectrum analogous to the Fourier energy spectrum. This requires assigning a Fourier frequency to each wavelet scale and normalizing both the Fourier and global wavelet spectrum (Torrence & Compo, 1998) (e.g., for the $n = 2$, Mexican hat, wavelet, this increases the minimum observed scale from $2 \times dt$ to $7.95 \times dt$). The further benefit of using a wavelet decomposition comes from the creation of the modulus maxima tree. At each scale, localized maxima in the modulus of the wavelet transform are identified. These are then connected across scales to

form maxima lines, essentially ridges identifying maxima across scale. There is always at least one WTMM line pointing towards any singularity (Mallat, 1998), $t_0$, and this scales as,

$$WT(t_0, a) \sim a^{h(t_0)+\frac{1}{2}} \ . \tag{3.30}$$

When singularities are well separated in time, this can be used to calculate the local Hölder exponent for each singularity (Struzik, 1998; Struzik, 2000). However, when singularities are not isolated, a global partitioning has to be introduced. Let $t_{mm}$ be all positions of local maxima of $|WT(t, a_0)|$ at some scale $a_0$, then define the partition function as the summation of the modulus of the wavelet coefficients to some power, $q$,

$$Z(q, a) = \sum_{mm} |WT(t_{mm}, a)|^q \ . \tag{3.31}$$

As before, the moment, $q$, plays the role of increasing the weighting of contribution of the largest wavelet transform coefficients to the summation when $q > 0$, and increasing the weighting of the smallest wavelet transform coefficients to the summation when $q < 0$. The approach of only including the modulus maxima removes very small values of the wavelet transform, which would otherwise cause divergence at $q < 0$. This also dramatically reduces the computational time, and incorporates the branch-like multiplicative structure of the wavelet transform into the partition function. Although the multifractal spectra may be calculated from this partition function, it is generally preferred to used the canonical approach (Chhabra & Jensen, 1989; Muzy et al., 1991) where,

$$u_{mm_i}(q, a) = \frac{|(WT(t_{mm_i}, a)|^q}{\sum_{mm_i} |WT(t_{mm_i}, a)|^q} \ , \tag{3.32}$$

is the effective Boltzmann weighting of each modulus maxima risen to $q$ at each scale. From this new measure,

$$h(q) + \frac{1}{2} = \lim_{a \to 0} \frac{1}{\log a} \sum_{mm_i} u_{mm_i}(q, a) \ \log \ |(WT(t_{mm_i}, a)| \ , \tag{3.33}$$

$$D(h(q)) = \lim_{a \to 0} \frac{1}{\log a} \sum_{mm_i} u_{mm_i}(q, a) \ \log \ (u_{mm_i}(q, a)) \ . \tag{3.34}$$

Equations 3.33 and 3.34 can be solved by a linear regression of the summation against the scale values ($log\ a$), and hence the singularity spectrum, $D(h)$, can be directly calculated at each $q$. The log-log plots of Equation 3.33 and 3.34 are generally linear, with more scatter about the linear trend at negative $q$. The major problem with the WTMM approach is in tracking the ridges correctly. Maxima in the wavelet may exist which do not correspond

to singularities; these ridges will not exist down to the very lowest scales. Tracking rules which are too relaxed will include these maxima, thereby contaminating the Boltzmann weightings in Equations 3.33 and 3.34. On the other hand, tracking rules which are too strict may not be able to follow the ridge to large enough scales; again this will affect the Boltzmann weightings in Equations 3.33 and 3.34. Another recent advance in this field uses the properties of the wavelet transform in order to overcome the limitations of the box counting method (Conlon et al., 2009; Kestener et al., 2010) by pre-selecting those modulus maxima corresponding to background noise and removing them before forming the multifractal spectrum.

## 3.5 Future directions

Since Mandelbrot first introduced the fractal dimension, the idea of quantitatively describing the complexity of a system (or an image of that system) has been applied in many areas of science. From a purely theoretical viewpoint, the fractal dimension is an indication of the self similarity of a shape across multiple size scales. We can conceptually consider multifractals as a conglomeration of fractals occupying the same point (in space, time, or both space and time). From a mathematical perspective, the links between SOC and fractal geometry are numerous - many SOC systems can be described by fractal geometry when described in appropriate phase space, any snapshot of an SOC system is likely to be fractal, and the long term dynamic evolution of an SOC system is likely to be fractal. The features that provide these connections are self-similarity (and scale invariance), power laws, the upper and lower limits to the scale-free range and the iterative methods used to generate both SOC models and fractals. It seems clear that fractal geometry provides one route to test our modern SOC models against real data. However, there are caveats - there is more than one fractal dimension and the techniques used to calculate fractal geometry are not all generally applicable. Recent advances in generating accurate and robust multifractal measures may provide a new tool to link models to data. Specifically, the incorporation of multiscale techniques (e.g., wavelets) may assist with the problems of spatial and temporal resolution. They also provide connections to theories in the areas of turbulence and magnetohydrodynamics that assist us in inferring physical parameters from unitless indices. The final argument for increasing research in this area of connecting fractal geometry and SOC may be that of a new data-driven approach to science. Our data volumes (from both models and experiments) and computational ability are increasing beyond the capabilities of an individual scientist and even an individual research field. The interdisciplinary ability to quantify features and classify images is set to become a vital tool in the scientists kit. Perhaps the links between fractal geometry and SOC can lead the way in these efforts.

## References

Abramenko, V.I., Yurchyshyn, V.B., Wang, H., Spirock, T.J., Goode, P.R. Scaling Behavior of Structure Functions of the Longitudinal Magnetic Field in Active Regions on the Sun, ApJ, 577, 487 (2002)

Alber, A., Peinke, J., An Improved Multifractal Box-Counting Algorithm, Virtual Phase Transitions, and Negative Dimensions (1997)

Arneodo, A., Bacry, E., Graves, P.V., Muzy, J.F., Characterizing long-range correlations in DNA sequences from wavelet analysis, Phys. Rev. Lett. 74, 3293 (1995)

Arneodo, A., Audit, B., Decoster, N., Muzy, J.F., Vaillant, C. Wavelet based multifractal formalism: Application to DNA sequences, satellite images of the cloud structure and stock market data in The Science of Disasters: Climate Disruptions, Heart Attacks, and Market Crashes (A. Bunde, J. Kropp, H. J. Schellnhuber, eds.), pp. 26-102. Springer Verlag, Berlin. (2002)

Balke, A. C., Schrijver, C. J., Zwaan, C., Tarbell, T. D. Percolation theory and the geometry of photospheric magnetic flux concentrations, Sol. Phys., 143, 215 (1993)

Bak, P., Tang, C., Wiesenfeld, K., Self-organized criticality: An explanation of the 1/f noise. Physical Review Letters 59 (4), 381, (1987)

Bovelet, B., Wiehr, E. A New Algorithm for Pattern Recognition and its Application to Granulation and Limb Faculae, Sol. Phys., 201, 13 (2001)

Cadavid, A.C., Lawrence, J.K., Ruzmaikin, A.A., Kayleng-Knight, A. 1994, ApJ, 429, 391

Conlon, P. A., Gallagher, P. T., McAteer, R. T. J., et al., Sol Phys, 248, 297 (2008)

Conlon, P.A., Kestener, P., McAteer, R.T.J., Gallagher, P.T., Fennel L., Khalil, A. Arneodo, AA (2009)

Chhabra, A., Jensen, R., Direct determination of the f(alpha) singularity spectrum, Physical Review Letter 62 (12), 13271330 (1989)

Clegg, Richard, A practical guide to measuring the Hurst parameter, ISSN 1473-804x online (2009)

Decoster, N., Roux, S.G., Arneodo, A. A wavelet-based method for multifractal image analysis. II. Applications to synthetic multifractal rough surfaces Eur. Phys. J. B 15, 739-764. (2000)

Evertsz, C.J.G., Mandelbrot, B.B., Multifractal measures in: Peitgen, H.-O., Jué rgens, H., Saupe, D. (Eds.), Chaos and Fractals. Springer-Verlag, New York, (1992)

Georgoulis, G.,Turbulence In The Solar Atmosphere: Manifestations And Diagnostics Via Solar Image Processing, 228, 5 (2005)

Gleick, James, Chaos, USA (1987)

Grassberger, P., Procaccia, I., Measuring the Strangeness of Strange Attractors. Physica D: Nonlinear Phenomena 9 (12), 189, (1983)

Hirzberger, J., V‡zquez, M., Bonet, A., Hanslmeier, A., Sobotka, M.. Time Series of Solar Granulation Images. I. Differences between Small and Large Granules in Quiet Regions, ApJ, 480, 406 (1997)

Hofstadter, Douglas, Gödel, Escher, Bach: An Eternal Golden Braid, Basic Books, USA (1970)

Hohenberg, Pierre, Dynamical theory of critical phenomena, in E. G. D. Cohen (Ed.) Statistical mechanics at the turn of the decade, Dekker, New York (1971)

Hilborn, R., Chaos and Nonlinear Dynamics: An introduction for Scientists and Engineers Oxford University Press, UK (2000)

Janssen, K., Všgler, A., Kneer, F., On the fractal dimension of small-scale magnetic structures in the Sun, AA, 409, 1127 (2003)

Kestener, P., Arneodo, A. Generalizing the wavelet-based multifractal formalism to random vector fields: Application to three-dimensional turbulence velocity and vorticity data Phys. Rev. Lett. 93, 044501 (2004)

Kestener, P. Conlon, P.A. Khalil, A., Fennell, L., McAteer, RTJ.,Gallagher, PT., Arneodo, A. Characterising Complexity in Compound Systems: Segmentation in Wavelet-Space, ApJ, 717, 995 (2010)

Kuhn, Thomas, The structure of scientific revolutions, USA (1967)

Lawrence, J. K. Diffusion of magnetic flux elements on a fractal geometry, Sol. Phys., 135, 249 (1991)

Lawrence, J.K., Ruzmaikin, A.A., Cadavid, A.C. 1993, ApJ, 417, 805

Lawrence, J.K., Cadavid, A.C., Ruzmaikin, A.A. On the Multifractal Distribution of Solar Magnetic Fields, ApJ, 465, 425 (1996)

Mandelbrot, Benoit B, The Fractal Geometry of Nature, San Francisco (1982).

Mandelbrot, Benoit B, Les objets fractals, forme, hasard et dimension, Paris, Flammarion (1975)

Mallat, S. G. A Wavelet Tour of Signal Processing, San Diego Academic, (1998)

McAteer, R.T.J., Gallagher, P.T, Ireland, J., Statistics of Active Region Complexity: A Large-Scale Fractal Dimension Survey, ApJ, 631, 628 (2005)

McAteer, R.T.J., Young, C.A., Ireland, J., Gallagher, P.T, The Bursty Nature of Solar Flare X-Ray Emission, ApJ, 662, 691 (2007)

McAteer, R.T.J., Gallagher, P.T., Conlon., P.A., Turbulence, complexity, and solar flares, Advances in Space Research, 45, 9, 1067 (2010)

Meunier, N. Fractal Analysis of Michelson Doppler Imager Magnetograms: A Contribution to the Study of the Formation of Solar Active Regions, ApJ, 515, 801 (1999)

Muzy, J.F., Bacry, E., Arneodo, A. Wavelets and multifractal formalism for singular signals: Application to turbulence data Phys. Rev. Lett. 67, 3515-3518, (1991)

Muzy, J.F., Bacry, E., Arneodo, A., Multifractal formalism for fractal signals: the structure fonction approach versus the wavelet transform modulus maxima method Phys. Rev. E 47, 875 (1993).

Newton, Isaac, Principia Mathematica, UK (1687)

Parisi, G., Frisch, U., On the singularity structure of fully developed turbulence in Turbulence and Predictability in Geophysical Fluid Dynamics (eds. M. Ghil, R. Benzi and G. Parisi). Proceedings of the International School of Physics ŇEnrico FermiÓ 8487, North-Holland. (1985)

PoincarŽ, Jules Henri, Sur le problŹme des trois corps et les Žquations de la dynamique. Divergence des sŽries de M. Lindstedt. Acta Mathematica, 13, 1270 (1890)

Roudier, Th., Muller, R. Structure of the solar granulation Sol. Phys., 107, 11 (1987)

Seuret, S., Gilbert, A. Proc. 13th ITC Specialist Seminar on Internet Traffic Measurement and Modelling (Paris: Int. Teletraffic Congr.) (2000), No. 14

Shaw, R. The Dripping Faucet As a Model Chaotic System, Science Frontier Express Series, Aerial Press, (1984)

Stark, B., Adams, M., Hathaway, D. H., Hagyard, M. J. Evaluation of Two Fractal Methods for Magnetogram Image Analysis Sol. Phys., 174, 297 (1997)

Struzik, Z. R. Removing Divergences in the Negative Moments of the Multi-Fractal Partition Function with the Wavelet Transformation, CWI Rep. INS-R9803, Amsterdam: Cent. Wiskunde Inf., (1998)

Struzik, Z. R., Siebes, A. P. J. M.. Outlier Detection and Localisation with Wavelet Based Multifractal Formalism, CWI Rep. INS-R0008, Amsterdam: Cent. Wiskunde Inf. (2000)

Swinney, H.L. and Gollub, J.P. Hydrodynamic Instabilities and the Transition to Turbulence, Physics Today, 1978

Taqqu, M., Teverovsky, V., Willinger, W. Estimators for long-range dependence: an empirical study, Fractals, 3, 785 (1995)

Torrence, C., Compo, G. P., Bull. Am. Meteorol. Soc., 79, 61 (1998)

Wolf, A, Swift, J. B, Swinney, H. L, Vastano, J. A. Determining lyapunov exponents from a time series. Physica D: Nonlinear Phenomena 16, 285317 (1985)
Winfree, A.T, The geometry of biological time, springer, new york (1980)
Vlahos, L, Georgoulis, M., Kluiving, R., Paschos, P., The statistical flare, AA, 289, 897 (1995)